Supporting Information

Enhancing CO_2 methanation over metal foam structured catalyst by electric internal heating

Liguang Dou,[‡a] Cunji Yan,*[‡a] Liangshu Zhong,[b] Dong Zhang,[a] Jingye Zhang,[a] Xin Li*[a] and Liye Xiao[a]

[a] Institute of Electrical Engineering, Chinese Academy of Sciences, No.6 Beiertiao, Zhongguancun, HaiDian District, Beijing, P.R. China.

[b] Shanghai Advanced Research Institute, Chinese Academy of Sciences, No.99 Haike Road, Zhangjiang Hi-Tech Park, Pudong Shanghai, P.R. China.

*Corresponding Author Email: yancj@mail.iee.ac.cn (C. Y) or drlixin@mail.iee.ac.cn (X. L)
‡ These authors contributed equally to this work.

Materials

Nickel foams (100 ppi) with a size of ca. 4 mm×70 mm×1.5 mm were purchased from Suzhou Jiashide Metal Foam Co. Ltd (Jiangsu, China). They were cleaned ultrasonically in a 6 M HCl solution for 5 min and washed with deionized water and absolute ethanol, before being dried in an oven at 60 °C. All chemical reagents were analytical grade and purchased from Aladdin Chemistry Co. Ltd (Shanghai, China). The deionized water with resistivity of >18.0 MΩ·cm was used throughout the experiments.

Characterization

Scanning electron microscopy (SEM) and energy dispersive X-ray spectroscopy (EDX) analyses were carried out on an Oxford Instruments INCAx-act EDX detector attached to a Zeiss Supra 55 field emission scanning electron microscopy. High-resolution transmission electron microscope (HRTEM) images were recorded on a JEOL JEM-2010 with an accelerating voltage of 200 kV. The high-angle annular dark-field scanning transmission electronmicroscopy (HAADF-STEM) images were recorded on a JEOL JEM-2100F transmission electron microscopy. X-ray diffraction (XRD) patterns were recorded on Bruke D8 Advance powder X-ray diffractometer using Cu-Kα source at 40 kV and 40 mA. The content of Ni was determined by inductively coupled plasma optical emission spectroscopy (ICP-OES, Optima 7000 DV, Perkin Elmer).

Experimental Procedures

Synthesis of the Ni foam structured catalysts

Typically, for NiAl-LDH/NF precursor, several pieces of treated Ni foams were used as the substrate for the growth of hierarchical flower-like NiAl-LDH plates. Briefly, the Ni foams were immersed into a solution of $Ni(NO_3)_2·6H_2O$ (0.009 mol), $Al(NO_3)_3·9H_2O$ (0.003 mol) and urea (0.04 mol) dissolved in 75 mL of deionized water in a Teflon-lined autoclave. The autoclave was sealed and heated at 110 °C for 8 h. The resultant product was washed with deionized water several times and dried at 65 °C for 12 h in air. The NiAl-LDH/NF derived monolithic catalyst was obtained via an in situ calcination-reduction process of the precursor in tube furnace at 500 ^oC for 3 h with a heating rate of 2 ^oC/min in a flowing H_2/N_2 stream (1/10, v/v). Black strip-shaped metal foams were obtained after the furnace was naturally cooled down to room temperature and the catalyst was denoted as Ni/NF. CoAl-LDH/NF (molar ratio of Co:Al=3:1) was also prepared via the similar procedures except for the addition of $Co(NO_3)_2·6H_2O$ and NH_4F. After calcination at 700 ^oC for 2 h, the derived catalyst was denoted as Co/NF. The load amount of LDH (ca. 10 mg) in the composite determined by the weight difference between LDH/NF precursor and pristine NF.

Trace amounts of noble metal Ru doped bimetallic catalysts were prepared by wet impregnation of

LDH/NF precursors in diluted $RuCl_3$ solution, followed by a calcination-reduction process. The Ru loading of 0.5 wt% was attempted for both the catalysts. Typically, RuNiAl-LDH/NF and RuCoAl-LDH/NF derived catalysts were denoted as RuNi/NF (500 ^oC, 3h) and RuCo/NF (700 ^oC, 2h), respectively.

Catalysis procedures

The experimental setup for catalytic hydrogenation of CO_2 using metal foam structured catalyst under electric internal heating (EIH) is shown in Fig. 1A. Both ends of metal strap first connected with copper wires using low electrical-resistivity copper terminals and then placed into a flow-type quartz tube reactor (200 mm length by 8 mm internal diameter) at atmospheric pressure. The quartz tube was connected to the electrically insulated propylene pipes by two vacuum connectors, and the copper wires as well as a thermocouple were sealed in the pipes by sealing washers embedded in reducing couplings to prevent leakage of gas during the reaction. A digital constant-current DC power supply with a resolution of 0.1 mA (CH-hall F2030; Beijing CuiHaiJiaCheng Technology) was used to impose the electric current to the metal foam structured catalysts. The voltage on the catalyst was monitored by a high precision digital multimeter (U1401B; Agilent technology). A sliding rheostat was connected in series in the circuit to protect the power supply. The reaction temperature was measured by an inserted K-type thermocouple closely attached to the surface of the catalyst and a infrared thermal imager with thermal sensitivity of 0.07 ^oC and an accuracy of ±2 ^oC (ST9450, Smart Sensor, Hong Kong, China) through the ZnSe window. The detailed temperature calibration curves for the K-type thermocouple and the IR imager were presented in Fig. S1.

Before the catalytic test, the catalyst was pre-treated in situ under 10% H_2-Ar mixture with flow rate of 30 mL/min at 250 ^oC for 0.5 h and then cooled to room temperature. Then, the mixed gas (CO_2/H_2/Ar=1/4/5) was introduced into the reactor with the same space velocity. The methanation activities of the catalysts were tested by applying varied currents into the circuit. The products were online quantified using a GC-FID (SP-3420A, Beijing Beifen-Ruili Analytical instrument (Group). CO., Ltd., China) with a Porapak-Q column for analyses of CH_4 and C_2H_6, and a GC-TCD with a TDX-01 column for analyses of Ar, CO, CH_4 and CO_2. Also, the changes of the reactants and products were monitored in real time using a quadrupole mass spectrometer (HPR-20, Hiden Analytical, Warrington, UK) equipped with a heated (453 K) fast response inlet capillary system. Finally, the CO_2 conversion (X_{CO2}) and CH_4 selectivity (S_{CH4}) were calculated by the Equation (1) and (2) (Ar is used as internal standard), and the increased activity in Fig.2 is defined as the percentage of the increased CO_2 conversion under EIH ($C_{CO_2,EIH} - C_{CO_2,CH}$) to the CO_2 conversion under CH ($C_{CO_2,CH}$), as shown in equation (3).

$$C_{CO_2}(\%) = \frac{F_{in}X_{CO_2,in} - F_{out}X_{CO_2,out}}{F_{in}X_{CO_2,in}} \times 100 = (1 - \frac{X_{Ar_2,in}X_{CO_2,out}}{X_{Ar,out}X_{CO_2,in}}) \times 100 \quad (1)$$

Where F_{in} and F_{out} indicate the total flow rate at inlet and outlet of the reactor; $X_{CO_2,in}$ and $X_{CO_2,out}$ indicate the concentration of CO_2 at inlet and outlet of reactor; $X_{Ar,in}$ and $X_{Ar,out}$ indicate the

concentration of Ar at inlet and outlet of reactor.

$$S_{CH_4}(\%) = \frac{F_{out}X_{CH_4,out}}{F_{in}X_{CO_2,in} - F_{out}X_{CO_2,out}} \times 100 \quad (2)$$

Where $X_{CH_4,in}$ and $X_{CH_4,out}$ indicate the concentration of CH_4 at inlet and outlet of the reactor.

$$\text{Increased activity}(\%) = \frac{C_{CO_2,\text{EIH}} - C_{CO_2,\text{CH}}}{C_{CO_2,\text{CH}}} \times 100 \quad (3)$$

For the conventional external heating method (CH), the methanation process was studied under the same catalytic conditions as above, except for the use of an electrical furnace for heating the reaction. The thermodynamic equilibrium values for CO_2 methanation reaction were calculated by HSC Chemistry 7.0 based on the Gibbs free energy minimization method.

To verify if there exist significant systematic error of reaction temperature between EIH and CH, the experiments on temperature differences between EIH and CH were conducted for different catalysts. Take Ni/NF as an example, Ni/NF exhibited CO_2 conversion of 7.7% at 200 °C under EIH and however, it only exhibited CO_2 conversion of 1.5% at 200 °C under CH. Finally, it is found that when the reaction temperature rises to 225 °C under CH, the CO_2 conversion rate of Ni/NF can reach to 7.7% and the temperature difference of Ni/NF at 200 °C is calculated as 25 °C. Then, the temperature difference of Ni/NF at 250 °C can be also tested. Similarly, the temperature differences for other three catalysts can be obtained and the results are plotted as shown in Fig. 2E and F. As a common sense, if the temperature deviate between EIH and CH at a fixed temperature (e.g. 200 °C) is a constant value (e.g. 20 °C), all the catalysts need to increase reaction temperature (20 °C) at CH to reach the same CO_2 conversion rate with respect to EIH reactor. However, if the temperature differences for different catalysts are not the same values, the systematic error of reaction temperature between EIH and CH reactors can be reasonably neglected.

Preparation of the sulphur poisoned catalysts

For sulphur-resistant experiments, the catalysts were reduced at 350 °C for 1h, then they were directly exposed to Ar gas together with 15 ppm and 50 ppm H_2S at 350 °C for 0.5 h and 3 h, respectively. After the catalysts were cooled to room temperature, their catalytic performances were evaluated and compared under the two heating modes (EIH and CH).

Calculations of reaction order and activation energy

Kinetic experiments were performed in the kinetic region in fixed-bed quartz reactor at ambient pressure with CO_2 conversion generally lower than 15%. The reaction orders with respect to CO_2(n_{CO_2}) and H_2(n_{H_2}) were determined in a series of tests at 200 °C. For n_{CO_2}, CO_2 partial pressure was varied between 0.033 atm and 0.1 atm while maintaining constant H_2 partial pressure (P_{H_2}=0.4 atm). The same procedure was followed to measure n_{H_2}, where P_{H_2} was varied from 0.2 atm to 0.4 atm at constant P_{CO_2} (0.1 atm). The concentration of Ar was varied accordingly in order to keep the total flow

at 60 mL/min. The n_{CO_2} and n_{H_2} were calculated by fitting the following power law rate equation (equation 4).

$$r = k(P_{CO_2})^{n_{CO_2}}(P_{H_2})^{n_{H_2}} \quad (4)$$

Where r is the CH_4 formation rate (mmol g^{-1} s^{-1}) and k represents the reaction rate constant.

The active energy (E_a) was calculated using Arrhenius equation (equation 5), and the catalytic reaction rate of the catalyst were obtained in the temperature range of 180-220 °C.

$$\ln k = \ln A - \frac{E_a}{RT} \quad (5)$$

Where k represents the rate constant and A is the temperature-independent Arrhenius factor; R is the gas constant (8.314 J K^{-1} mol^{-1}) and T is the absolute temperature (K).

The reaction rate (r) was calculated from the experimental data by equation (6):

$$r = \frac{F_{CO_2\ in} \times X_{CO_2}}{W} = \frac{X_{CO_2}}{W / F_{CO_2\ in}} \quad (6)$$

Where $F_{CO_2,\ in}$ is mole flow rate of CO_2 at the inlet (mol/s), X_{CO_2} is the conversion of CO_2, W is the weight of catalyst (g).

Calculations of Energy efficiency

The total efficiency of the process to convert electrical energy into chemical energy is calculated by dividing the power carried by the CH_4 flow by the power carried by the H_2 flow plus the power required by the reactor (equation 7).

$$\eta(\%) = \frac{P_{CH_4}}{P_{H_2} + P_{inject}} \times 100 \quad \text{.....(7)}$$

Where η (%) represents the total energy efficiency and P_{inject} (W) is inject electric power during hydrogenation process; P_{CH4} and P_{H2} are defined as the power carried by the CH_4 flow and the H_2 flow, respectively. H_2 and CH_4 can be characterized by their superior calorific power (*PCS*) which represents the amount of energy generated by burning 1 mg of these gases, and CO_2 has no PCS since it can't be burnt (Table S2).

In the case of the Sabatier reaction efficiency, denoted as E (%), it can be seen as the amount of energy carried by the CH_4 flow produced as compared to the amount of energy carried by the flow H_2. The total energy efficiency (η) and the Sabatier reaction efficiency at 300 °C under EIH and CH are listed in Table S3.

Supporting Figures

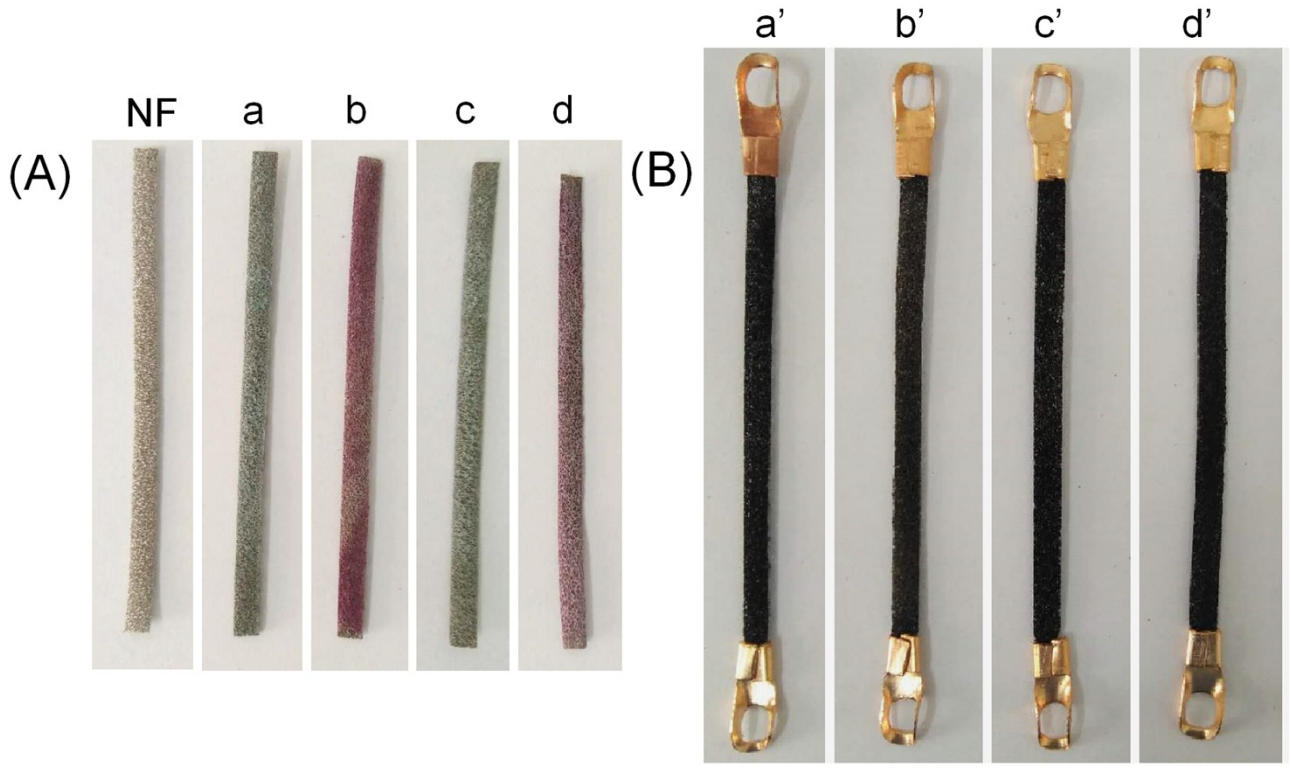

Figure S1 (A) Photographs of the precursors for NiAl-LDH/NF (a), CoAl-LDH/NF (b), RuNiAl-LDH/NF (c) and RuCoAl-LDH/NF (d). (B) Photographs of the derived structured catalysts for Ni/NF (a'), Co/NF (b'), RuNi/NF (c') and RuCo/NF (d').

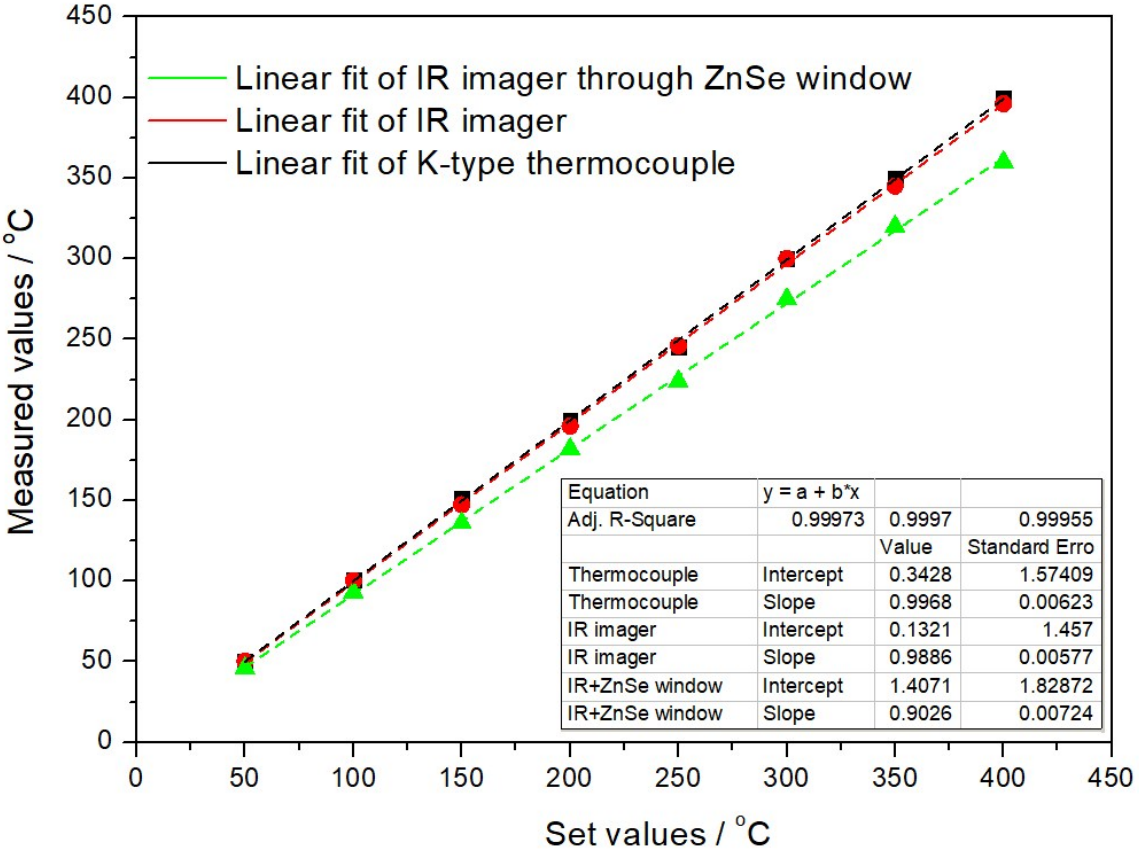

Equation	y = a + b*x		
Adj. R-Square	0.99973	0.9997	0.99955
		Value	Standard Erro
Thermocouple	Intercept	0.3428	1.57409
Thermocouple	Slope	0.9968	0.00623
IR imager	Intercept	0.1321	1.457
IR imager	Slope	0.9886	0.00577
IR+ZnSe window	Intercept	1.4071	1.82872
IR+ZnSe window	Slope	0.9026	0.00724

Figure S2 Temperature calibration curves for K-type thermocouple, IR imager and IR imager through a ZnSe window (2 mm in thickness).

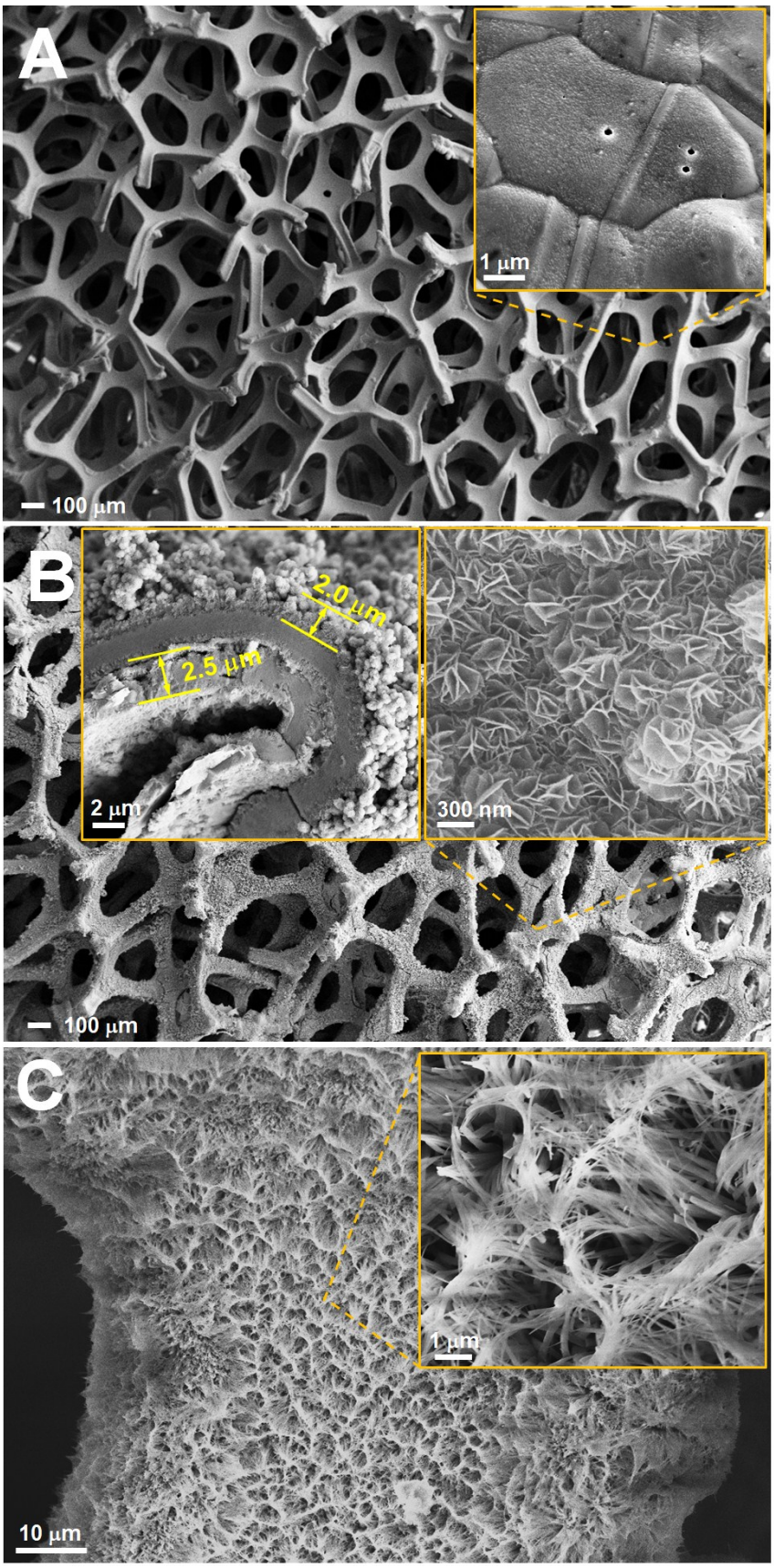

Figure S3 Low-magnification SEM images of (A) Ni foam, (B) NiAl-LDH/NF, (C) CoAl-LDH/NF. Insets are their enlarged images.

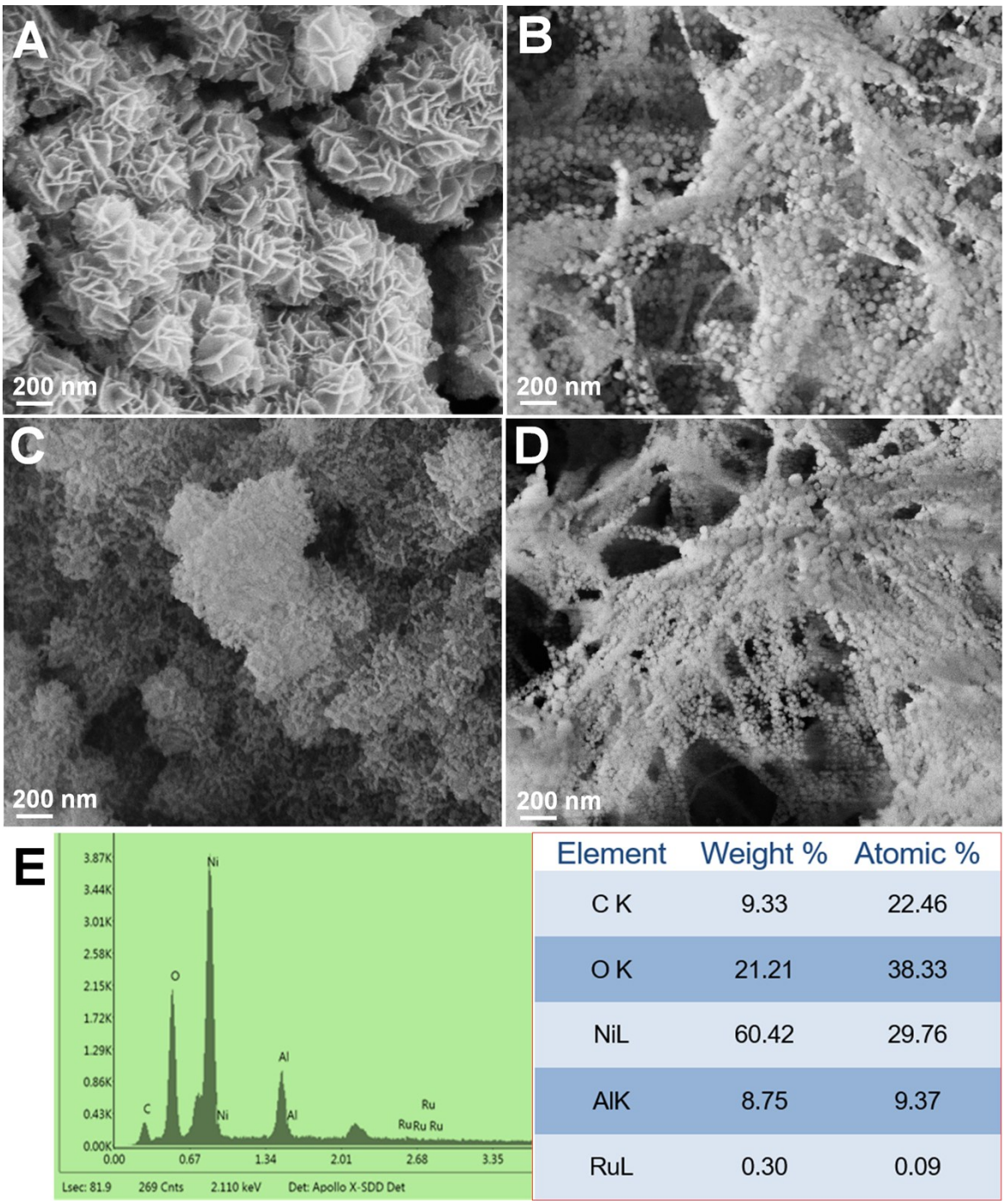

Element	Weight %	Atomic %
C K	9.33	22.46
O K	21.21	38.33
NiL	60.42	29.76
AlK	8.75	9.37
RuL	0.30	0.09

Figure S4 High-magnification SEM images of the catalysts (A) Ni/NF, (B) Co/NF, (C) RuNi/NF and (D) RuCo/NF; (E) is the EDX analyses of RuNi/NF.

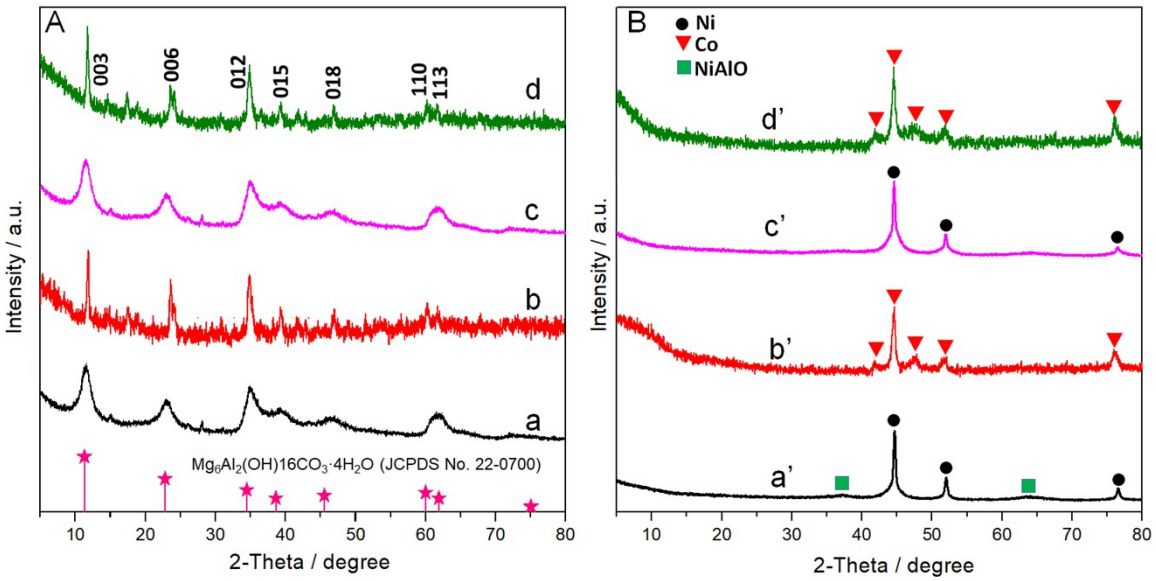

Figure S5 Power XRD patterns of (A) LDH precursors and (B) the derived catalysts scraped from the NF substrate. (a: NiAl-LDH/NF, b: CoAl-LDH/NF, c: RuNiAl-LDH/NF, d: RuCoAl-LDH/NF; a': Ni/NF , b': Co/NF, c': RuNi/NF, d': RuCo/NF)

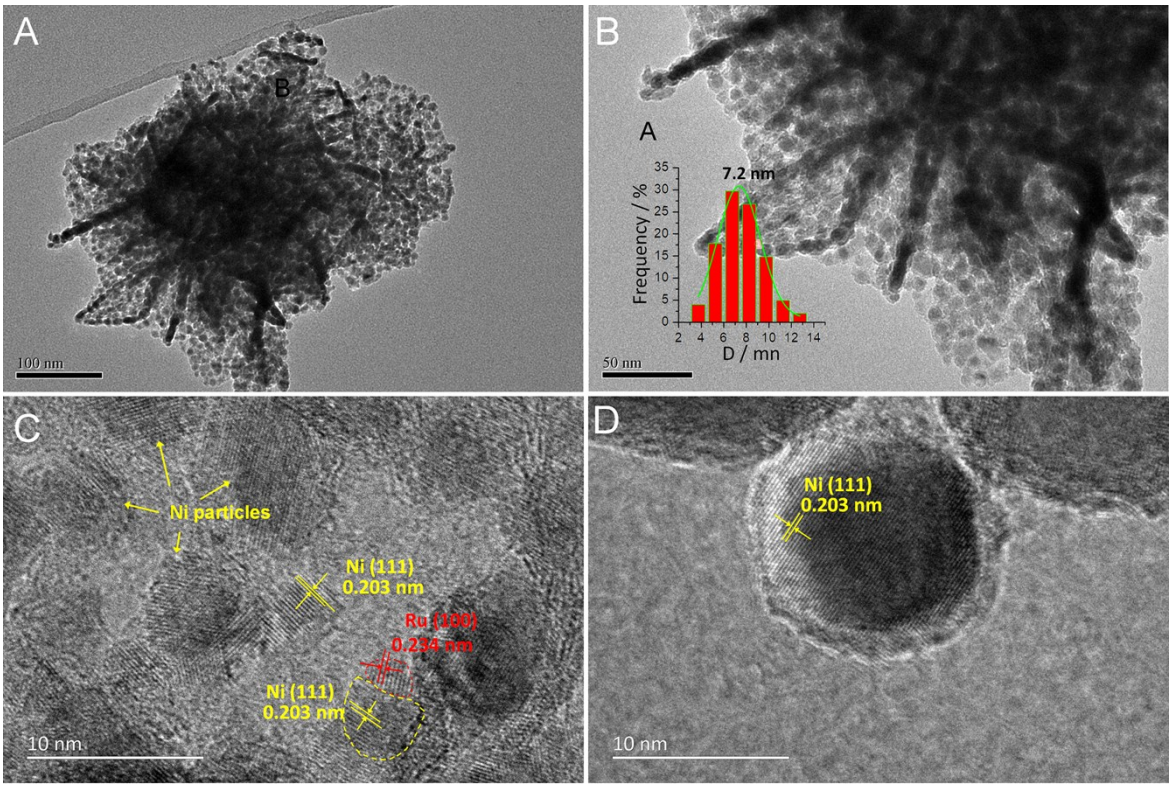

Figure S6 Typical (A, B) TEM and (C, D) HRTEM images for RuNi/NF catalyst.

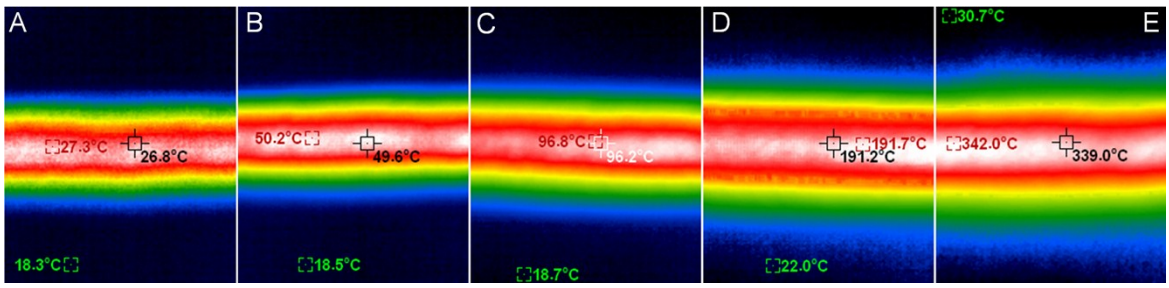

Figure S7 IR thermal images of RuNi/NF catalyst at varied temperatures during the electric internal heating process.

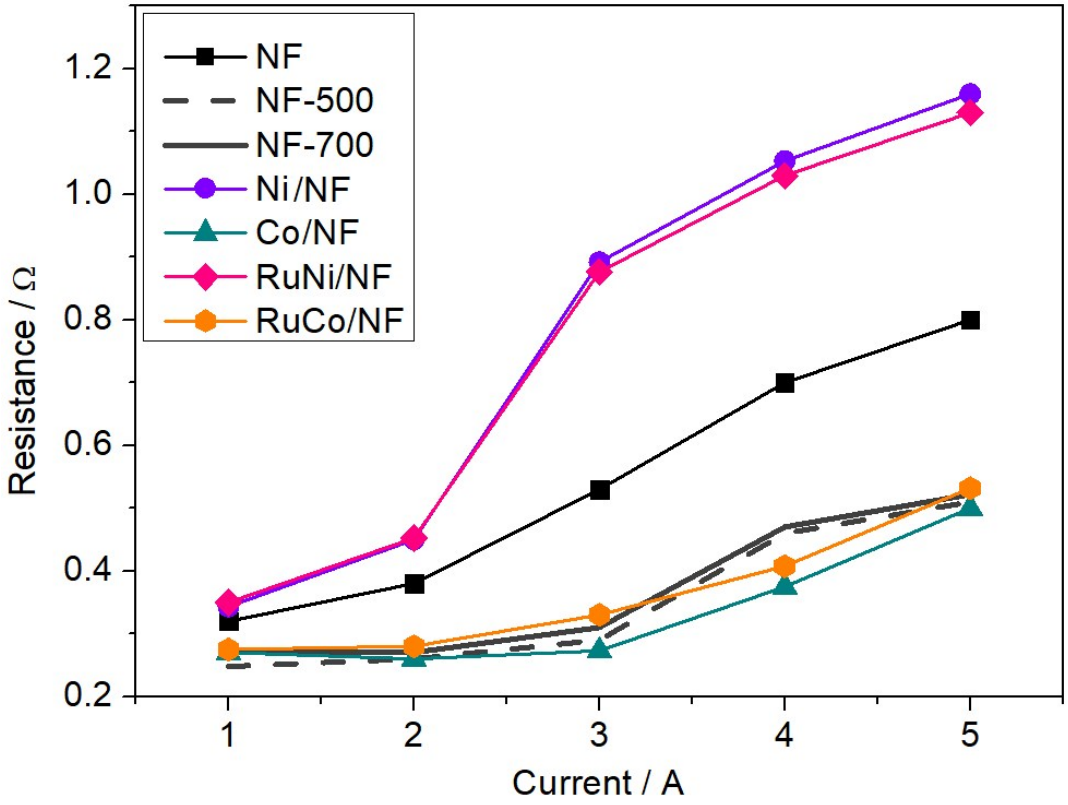

Figure S8 Electrical resistances under EIH as a function of the applied currents. (NF-500 and NF-700 were obtained from nickel foam calcining at 500 °C and 700 °C, respectively.)

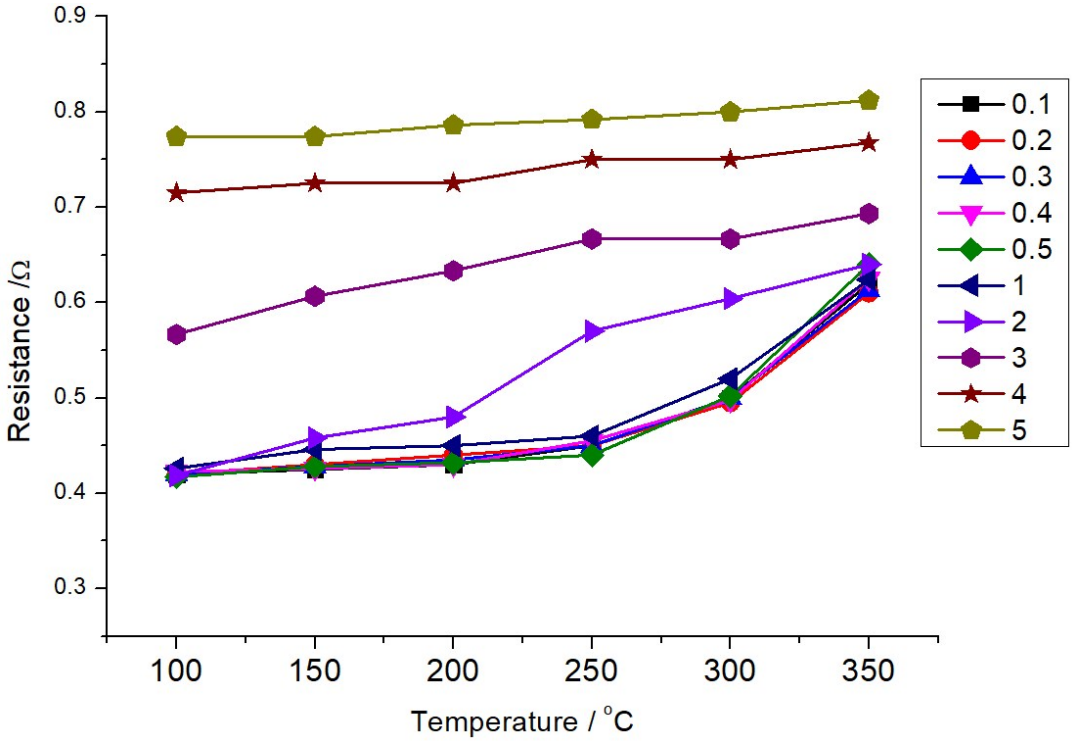

Figure S9 Electrical resistance changes of RuNi/NF by applying different currents (0.1, 0.2, 0.3, 0.4, 0.5, 1, 2, 3, 4 and 5 A) under a series of fixed reaction temperatures.

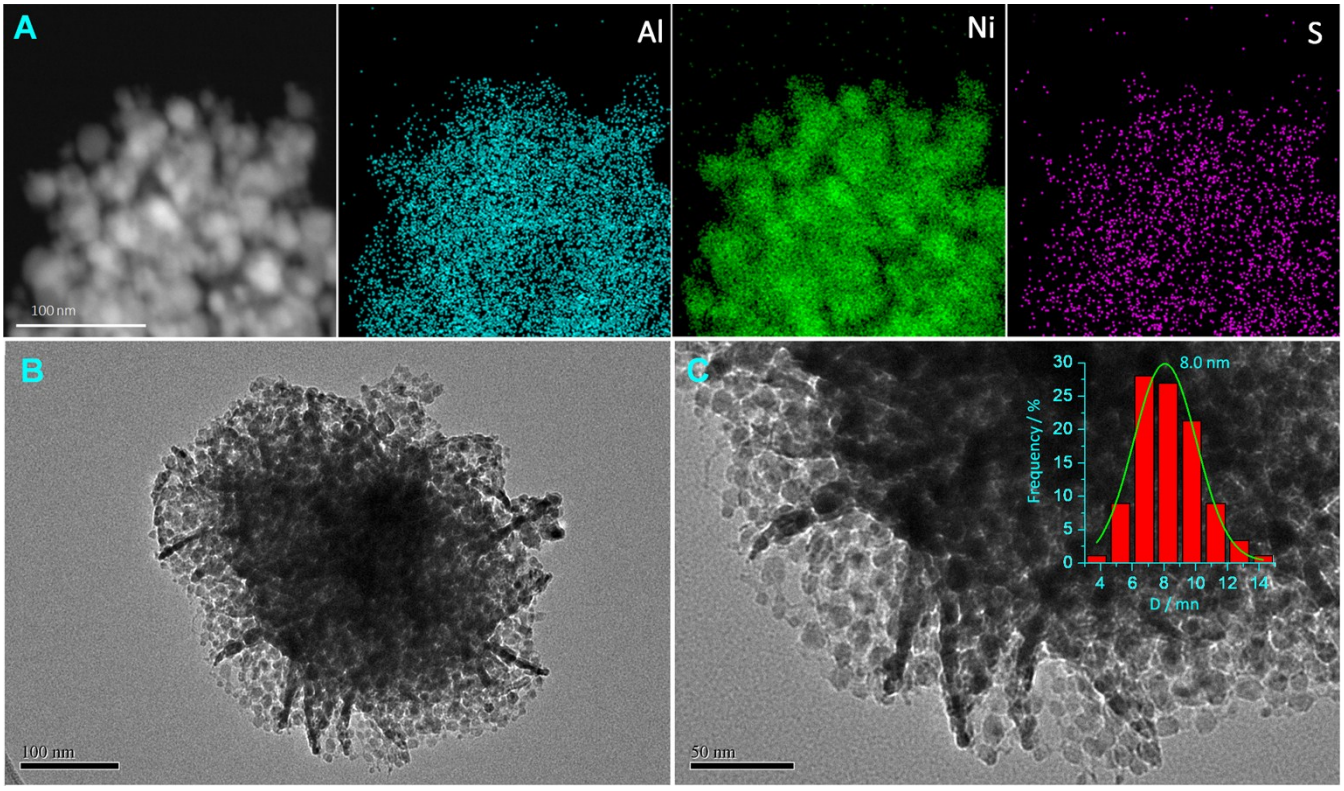

Figure S10 (A) HAADF mappings and (B, C) TEM image of the sulfur-poisoned RuNi/NF (50 ppm H_2S in Ar, 60 mL/min, 350 °C, 3 h).

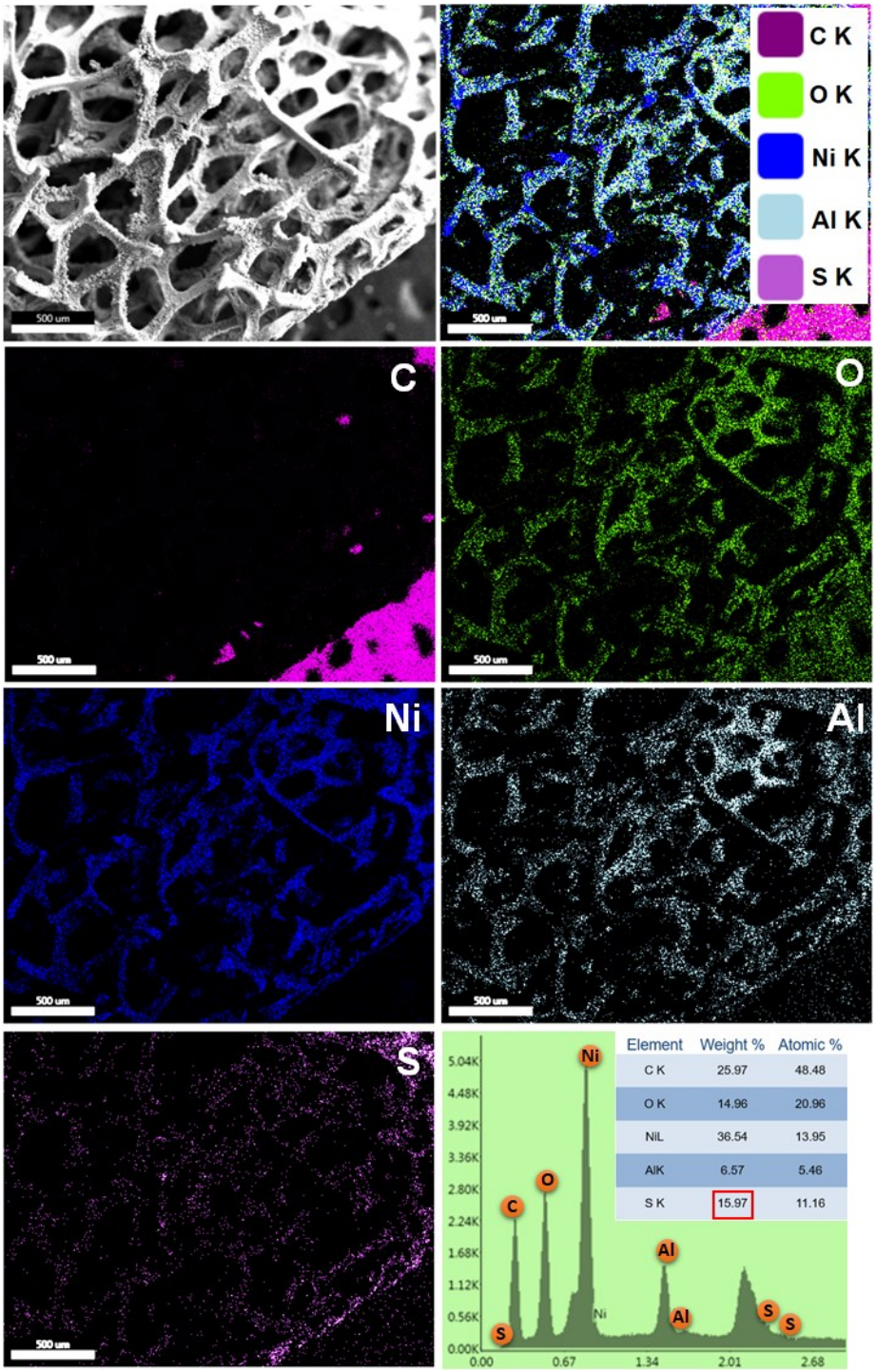

Figure S11 Typical SEM-EDX mapping analyses of the sulphur-poisoned catalyst RuNiAl/NF (50 ppm H_2S in Ar, 60 mL/min, 350 ^oC, 3 h).

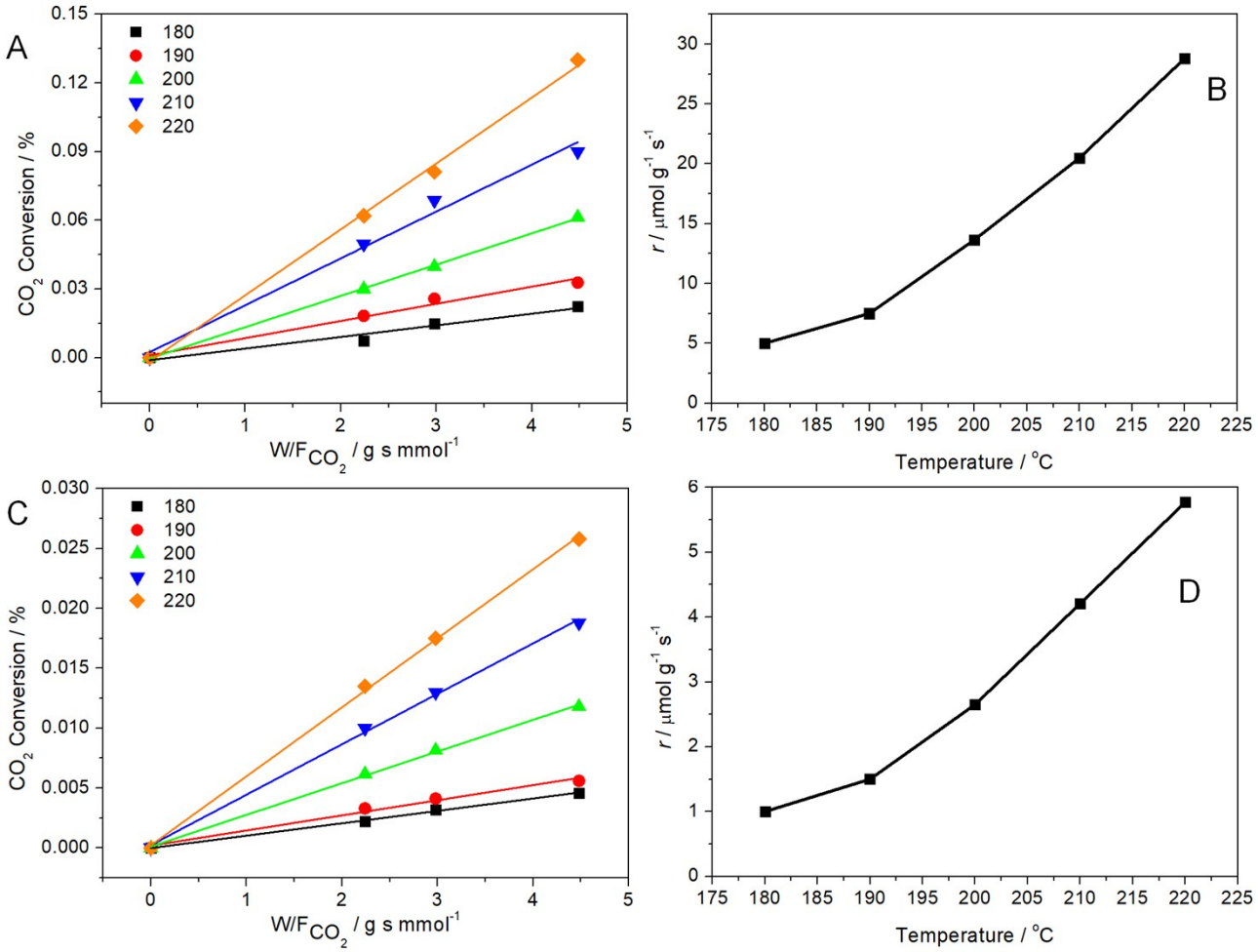

Figure S12 (A, C) Variation of fractional conversion of CO_2 with W/F_{CO_2} and (B, D) the reaction rate as a function of temperature (180-220 °C) for RuNi/NF catalyst under the EIH (A, B) and CH (C, D) modes.

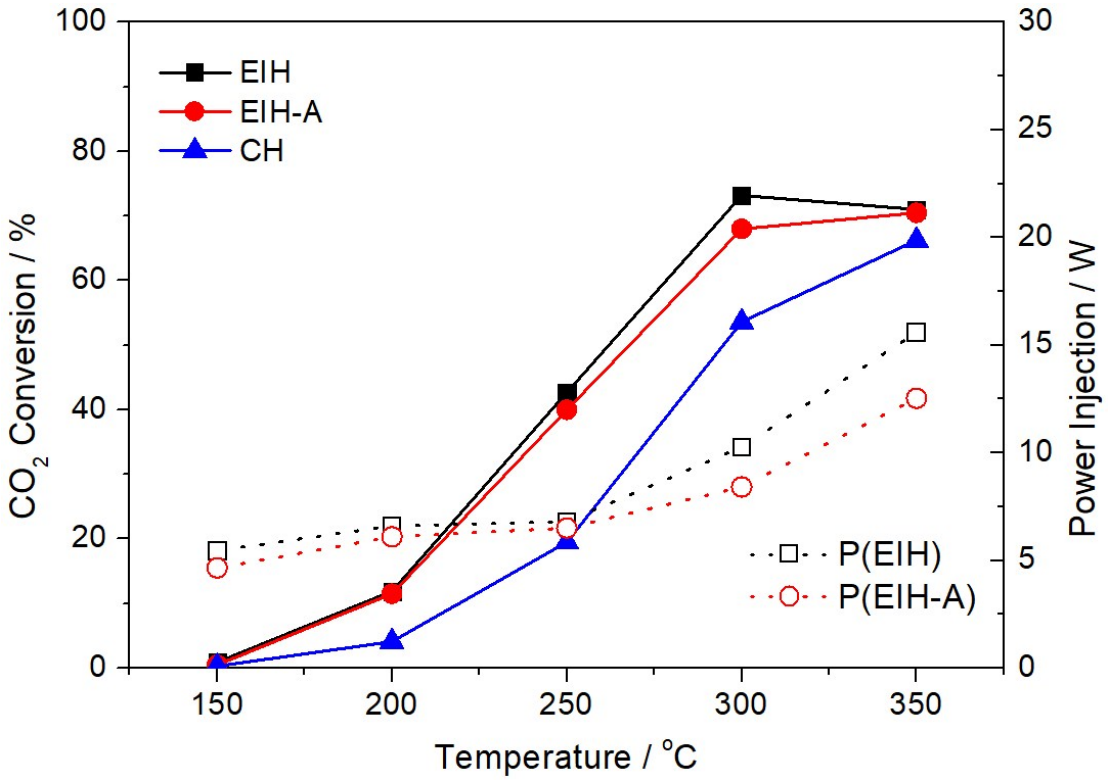

Figure S13 CO_2 conversion over RuNi/NF at various temperatures under EIH without thermal insulation, EIH with thermal insulation (EIH-A) and CH modes. The heat-insulating EIH reactor, wrapped with heat-preservation glass fiber felt with a thickness of 5 mm, only shows decreased power injection with nearly the same CO_2 conversion versus EIH without thermal insulation layer, indicating that the significantly enhanced CO_2 methanation activities under EIH with respect to conventional CH is not associated with its strengthened heat-transfer ability to the surroundings.

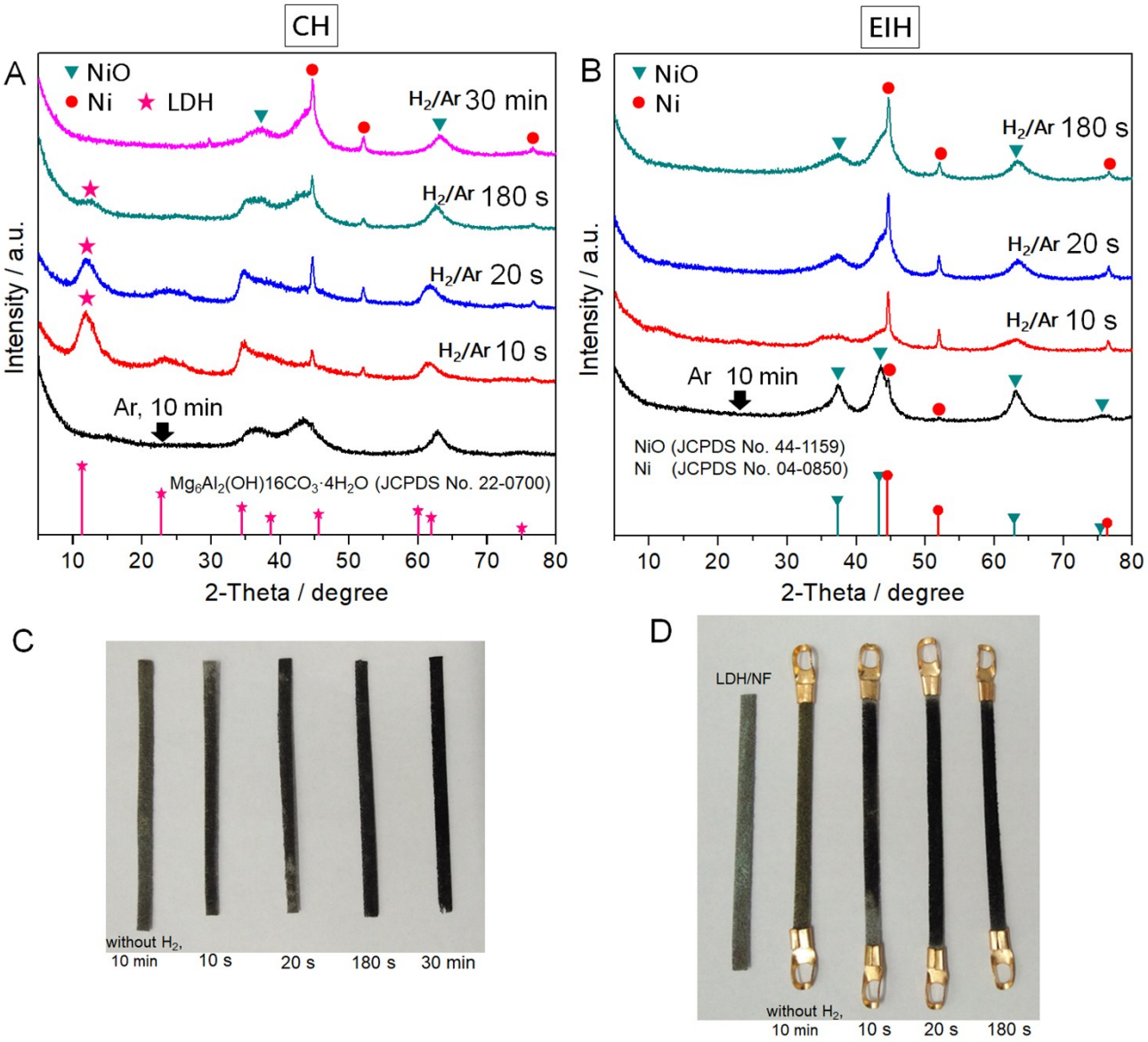

Figure S14 XRD patterns of heat-treated NiAl-LDH/NF precursor at 300 °C under (A) CH and (B) EIH heating modes with Ar and 50 vol%H_2/50 vol%Ar feed gas at a flow rate of 30 mL/min, respectively. (C) and (D) are the photographs of the used samples under CH and EIH, respectively.

The experiments of heat treatment (at 300 °C) under certain atmosphere (Ar and H_2/Ar) were designed to understand the difference between EIH and CH by observing the structure changes of the treated samples. The freshly prepared NiAl-LDH/NF (precursor of the catalyst) sample was used for these tests.

As shown in Figure S14A, heat treatments under Ar at 300 °C under conventional external heating (CH) for 10 minutes lead to dehydration, followed by dehydroxylation and decomposition of anions localized in the interlayers, resulting in the formation of NiO crystalline phase with typical diffractions at 37.3° (111), 43.2° (200) and 62.7° (220) (JCPDS

44-1159), consistent with previous results on transition metal Co substituted CoAl-LDH calcined in inert N_2 atmosphere (J. Pérez-Ramírez et al., *J. Mater. Chem.*, 2001, 11, 821). When H_2/Ar gas mixture (50%/50%) is used under CH, characterization peaks at 44.8° (111) and 52.1° (200) of metallic Ni (JCPDS 04-0850) are determined and its peak intensity increases with the increase of the treatment time. As a result, LDH, NiO and Ni phases co-exist in the H_2 treated samples (less than 180 s) under CH. When the treatment time increases to 30 minutes, the LDH phase completely disappears and the peak intensity of Ni (111) at 44.8° greatly increases, along with obvious NiO peak, indicating that the complete phase transformation of NiO to metallic Ni requries much higher reduction temperature.

As shown in Figure S14B, the reduction process of LDH phase to metallic Ni is significantly accelerated in EIH in comparison with CH. Typically, almost no LDH phase are observed for all the samples under EIH, even for the sample with a H_2 reduction duration of 10 s, indicating an obvious promotion effect on the H_2 reduction process. Furthermore, unlike the behavior under CH, another evidence related to the electronic effect of EIH is the appearance of Ni peaks in fully inert Ar atmosphere, although much lower in intensity, implying that the thermal electrons arising from EIH can promote the reduction of the Ni^{2+} ions in the LDH lattice to Ni.

Table S1: Electrical parameters applying on RuNi/NF for CO_2 methanation.

T/°C	Current/A	Voltage/V	Resistance/Ω	Power[a] /W
150	3.10	1.76	0.567	5.456
200	3.25	2.03	0.625	6.597
250	3.30	2.06	0.625	6.798
300	3.40	3.02	0.888	10.26
350	4.00	3.9	0.975	15.60

[a] Power (W) = Applied current (A) ×Applied voltage (V).

Table S2 Characteristics of the gas flows in the reactor at 300 °C under EIH.

Gas	*PCS* / J·mg^{-1}	Flow rate / mL·min^{-1}	*F*[a] / mmol·min^{-1}	M[b] / mg·min^{-1}	*PCS*·M / J·min^{-1}	P_{H_2} / W	P_{CH_4} / W
H_2(in)	120	12	0.48	0.96	115.2	1.92	-
CO_2(in)	-	3	0.12	5.28	-	-	-
CH_4(out)	50	2.185[c]	0.096	1.54	77	-	1.28

[a] *F*: molar feed rate.
[b] *M*: mass flow rate.
[c] F_{CH_4} : the flow rate of CH_4, calculated as $F_{CH_4}(\mathrm{ml/min}) = F_{CO_2}(\mathrm{mL/min}) \times X_{CO_2}(\%) \times S_{CH_4}(\%)$.

Table S3 Summary of the total energy efficiency (η) and the Sabatier reaction efficiency (E) under different heating methods.

Types	P_{H_2} / W	P_{CH_4} / W	P_{inject} /W	E[a] / %	η / %
EIH	1.92	1.28	10.26	66.8	10.5
CH	1.92	0.94	~40	48.9	~2.2
Magnetic induction ($Fe_{2.2}C$)[ref 1.]	8.1	15.1	-	78.1	~10

[a] The maximum energy efficiency, $E_{max}(Y_{CH_4})$, of the Sabatier reaction is calculated as 83.1% (CO_2:H_2=1:4, X_{CO_2}=100%, S_{CH_4}=100%).

As a result, it can be seen that the total energy efficiency (10.5%) and the Sabatier reaction efficiency (66.8%) at 300 °C over RuNi/NF under EIH are significantly higher than those under CH (~2.2% and 48.9%, respectively), and even comparable with those of the composite iron carbide nanoparticls under magnetic induction technique (Bordet, *Angew. Chem. Int. Ed.,* 2016, 55, 1).

Table S4: Comparison of the catalytic hydrogenation activities of the RuNi/NF and related catalysts.

Catalysts	Temperature /°C	Flow rate /ml·min^{-1}	Catalyst usage /mg	CO_2/H_2/Inert	X_{CO_2} /%	R_{CH_4}[a] /mmol·g^{-1}·h^{-1}	TOF[b] /s^{-1}	Refs.
RuNi/NF-EIH	300	30	~7	3/12/15	73.2	840.3	0.021	This work
RuNi/NF-CH	300	30	~7	3/12/15	53.6	615.3	0.015	This work
15Ni/Al_2O_3	250	100	100	1/24/0	-[c]	3.85	0.013	Ray et al.[2]
Ni/CeO_2	340	36.67	100	10/46/44	98.1	98.2	-	Zhou et al.[3]
10Co/ZrO_2	400 (3 MPa)	60	1000	1/4/0	92.5	29.7	0.2	Li et al.[4]
75Ni25Fe/Al_2O_3	250	100	100	1/24/0	-	12.2	0.034	Ray et al.[2]
20Ni/Al_2O_3-ZrO_2	300	50	500	1/4/0	77	41.3	-	Lin et al.[5]
10Ni-10La_2O_3/Na-BETA	350	250	500	4/16/5	65	139.3	-	Quindimil et al.[6]
Ru@FL-LDHs	~350	25.5	150	20.5/5/0	96.6	277	-	Ren et al.[7]
NiRu-CaO-Al_2O_3	380 (0.1 MPa)	100	200	3/12/5	83.8	168.3	-	Liu et al.[8]
5%Ru/Al_2O_3	300	60	-	1/4/0	<5.5	-	0.068	Wang et al.[9]
5%Ru/CeO_2	300	-	202	4.6/22/Ar	83	-	0.15	Dreyer et al.[10]

[a] R_{CH_4}: CH_4 formation rate, the moles of CH_4 produced per gram of catalyst per hour.
[b] TOF: the turnover frequency, the number of CO_2 molecules converted per mole of active component (Ni, Ru, Co etc.) per second. The measured bulk Ni content in the structured catalysts of this work is 66.69 wt.%.
[c] - : No data presented or calculated.

As summarized in Table S4, RuNi/NF-EIH(840.3 mmol•g^{-1}•h^{-1}, 0.021 s^{-1}) exhibits greatly higher CH_4 formation rate than RuNi/NF-CH (615.3 mmol•g^{-1}•h^{-1}, 0.015 s^{-1}), Ni/Al_2O_3 (3.85 mmol•g^{-1}•h^{-1}, 0.013 s^{-1}), Ni/CeO_2 (98.2 mmol•g^{-1}•h^{-1}), Al_2O_3 supported NiFe binary alloy (12.2 mmol•g^{-1}•h^{-1}), Ni/Al_2O_3-ZrO_2 (41.3 mmol•g^{-1}•h^{-1}), exfoliated LDHs loaded Ru nanoparticles (277 mmol•g^{-1}•h^{-1}) and NiRu-CaO-Al_2O_3 system (168.3 mmol•g^{-1}•h^{-1}), and lower than Co/ZrO_2 (0.2 s^{-1}) tested under 3

MPa at 400 °C and Ru-based catalysts (Ru/Al_2O_3 and Ru/CeO_2) with high noble metal loading (5 wt.%).

References

1. A. Bordet, L. M. Lacroix, P. F. Fazzini, J. Carrey, K. Soulantica and B. Chaudret, *Angew. Chem. Int. Edit.*, 2016, **55**, 15894-15898.
2. K. Ray and G. Deo, *Appl. Catal. B*, 2017, **218**, 525-537.
3. G. Zhou, H. Liu, K. Cui, A. Jia, G. Hu, Z. Jiao, Y. Liu and X. Zhang, *Appl. Surf. Sci.*, 2016, **383**, 248-252.
4. W. Li, X. Nie, X. Jiang, A. Zhang, F. Ding, M. Liu, Z. Liu, X. Guo and C. Song, *Appl. Catal. B*, 2018, **220**, 397-408.
5. J. Lin, C. Ma, Q. Wang, Y. Xu, G. Ma, J. Wang, H. Wang, C. Dong, C. Zhang and M. Ding, *Appl. Catal. B*, 2019, **243**, 262-272.
6. A. Quindimil, U. De-La-Torre, B. Pereda-Ayo, J. A. González-Marcos and J. R. González-Velasco, *Appl. Catal. B*, 2018, **238**, 393-403.
7. J. Ren, S. Ouyang, H. Xu, X. Meng, T. Wang, D. Wang and J. Ye, *Adv. Energy Mater.*, 2017, **7**, 1601657.
8. Q. Liu, S. Wang, G. Zhao, H. Yang, M. Yuan, X. An, H. Zhou, Y. Qiao and Y. Tian, *Int. J. Hydrogen Energy*, 2018, **43**, 239-250.
9. X. Wang, Y. Hong, H. Shi and J. Szanyi, *J. Catal.*, 2016, **343**, 185-195.
10. J. A. H. Dreyer, P. Li, L. Zhang, G. K. Beh, R. Zhang, P. H. L. Sit and W. Y. Teoh, *Appl. Catal. B*, 2017, **219**, 715-726.